J Mater Sci (2008) 43:1228–1233
DOI 10.1007/s10853-007-2264-8

ESR investigations on polyethylene-single wall carbon nanotube composites

Mircea Chipara · K. Lozano · Richard Wilkins · E. V. Barrera · M. X. Pulikkathara · Laura Penia-Para · Magdalena Chipara

Received: 26 May 2007 / Accepted: 26 October 2007 / Published online: 4 December 2007
© Springer Science+Business Media, LLC 2007

Abstract Electron spin resonance investigations on single wall carbon nanotubes dispersed in polyethylene are reported. Three resonance lines were observed; a wide line assigned to magnetic iron clusters (catalyst residues), a broad and intense line originating from uncoupled electrons delocalized over the conducting domains of carbon nanotubes (in interaction with the electronic spins assigned to magnetic impurities), and a faint line superimposed on the broad one, assigned to paramagnetic impurities. The temperature dependence of resonance line parameters (resonance line position, width, and double integral) in the range 150–450 K has been analyzed. It was observed that the parameters of the broad and narrow lines are sensitive to the glass and melting relaxations occurring within the polymeric matrix.

M. Chipara (✉) · M. Chipara
Department of Physics and Geology, University of Texas Pan-American, 1201 W. University Drive, Edinburg, TX 78541-2999, USA
e-mail: mchipara@utpa.edu

K. Lozano
Department of Mechanical Engineering, University of Texas Pan-American, Edinburg, TX, USA

R. Wilkins
NASA Center for Applied Radiation Research, Prairie View A&M University, Prairie View, TX 77446, USA

E. V. Barrera · M. X. Pulikkathara · L. Penia-Para
Department of Mechanical Engineering and Material Science, Rice University, Houston, TX 77005, USA

Introduction

The amazing mechanical [1–4], thermal [4–7], and electric properties [8, 9] of carbon nanotubes along with their reduced density triggered much research; a major fraction of this research is now focused on the projection of the unmatched nanometer scale properties of carbon nanotubes to micron scale, and finally to the macroscale [3, 4]. Most of these investigations concentrated on polymer–carbon nanotube composites. While the filling of polymeric matrices with carbon nanotubes resulted in important improvements of the mechanical, thermal, and electric properties, most of these changes are below theoretical expectations. Functionalization of carbon nanotubes and in situ polymerization reactions are expected to result in a better anchoring and wrapping of polymeric chains around carbon nanotubes. The possibility to control and estimate the distribution of carbon nanotubes within polymeric matrices is expected to further increase the physical properties of polymer carbon nanotube composites [10].

Electron spin resonance (ESR) has been utilized to identify, analyze, and characterize carbon nanotubes (CNT) [11–18]. The typical ESR spectrum of CNT consists of three lines [11–18]. The low field (large g-value) wide line has been assigned to catalyst residues [11–15]. The narrow resonance line located close to the free electron g-value ($g = 2.0023$) has been assigned to amorphous carbon or graphite residues [13, 14]. The broad resonance line located near $g = 2.0023$ has been assigned to conducting electrons residing on single wall carbon nanotubes (SWNT) [13, 14].

Although many ESR investigations on carbon nanotubes have been reported [11–21], few ESR studies on carbon nanotubes dispersed in polymeric matrices were published [14, 17]. We report on the temperature dependence of ESR

line parameters of (SWNT) dispersed in high-density polyethylene (HDPE).

Experimental method

SWNTs were prepared by the HiPco process based on iron catalysts. Details concerning the growth of SWNTs and their dispersion within HDPE have been reported elsewhere [22]. Composites containing 5% SWNT in HDPE (HDPE–SWNT) have been investigated by using a Bruker ESP 300 spectrometer operating in X band (about 9 GHz). The temperature dependence of resonance spectra in the range 150–450 K has been investigated. The thermal characteristics of HDPE purchased from Aldrich are; glass transition temperature (T_{GHDPE}) at about 148 K and melting transition temperature at 403 K (T_{MHDPE}) [22].

Experimental results and discussions

To analyze accurately the shape of the ESR spectra, and to determine precisely the parameters of the resonance spectra such as line intensity, line position (resonance field or g factor), linewidth, and double integral of the resonance spectra, every ESR spectrum has been fitted by a convolution of three pure Lorentzian lines. Base line corrections up to the second-order were considered.

$$I(H) = I_1 \frac{\left(\frac{H-H_{R1}}{H_{PP1}}\right)}{\left[1+\left(\frac{H-H_{R1}}{H_{PP1}}\right)^2\right]^2} + I_2 \frac{\left(\frac{H-H_{R2}}{H_{PP2}}\right)}{\left[1+\left(\frac{H-H_{R2}}{H_{PP2}}\right)^2\right]^2} + I_3 \frac{\left(\frac{H-H_{R3}}{H_{PP1}}\right)}{\left[1+\left(\frac{H-H_{R3}}{H_{PP3}}\right)^2\right]^2} + C_0 + C_1 H + C_2 H^2 \quad (1)$$

where I_1, I_2, and I_3 are the intensities of the three resonance lines; H_{pp1}, H_{pp2}, and H_{pp3} are the linewidths of the three lines; H_{R1}, H_{R2}, and H_{R3} are the resonance line positions for the three lines; and C_0, C_1, and C_2 are fitting constants.

Carbon nanotubes exhibit typically an ESR spectrum consisting of three lines [14]:

1. A wide line located at low magnetic fields (high g values), assigned to magnetic impurities (catalyst residues). The position of this line shifts slowly toward lower magnetic field as the temperature of the sample is decreased. This derives from the fact that the position of the ESR line in magnetically ordered systems is controlled by the total magnetic field experienced by the uncoupled electronic spin (which includes both the local "molecular" magnetic field and the external applied magnetic field).
2. A broad, intense, and asymmetric line located near $g = 2.0$, assigned to electrons delocalized over carbon nanotubes. The asymmetry of the resonance line reflects the damping of the microwave field within nanotubes due to the skin effect. Theoretically, the double integral of this line should be temperature independent.
3. A weak and narrow resonance line, assigned to paramagnetic impurities, frequently hidden within the intense broad resonance line. The double integral of this line has a strong (Curie-like) dependence on temperature. Actually, the double integral of this line at liquid nitrogen should be about four times greater than the double integral of the same line at room temperature.

The ESR spectrum of SWNTs (not dispersed within the polymeric matrix) shows all these three resonances. The asymmetry of the broad resonance line at room temperature was low, suggesting a low electrical conductivity and a reduced number of contacts between nanotubes. The broad resonance line, at room temperature is located at $g = 2.071 \pm 0.0005$. The shift of the resonance line position (for the line assigned to electrons delocalized over carbon nanotubes) from the theoretical value ($g = 2.0023$) is generally assigned to the spin-orbit coupling and to the random orientation of carbon nanotubes. Such contribution may explain only shifts in the g-factor up to about 0.03. The observed large value of the g-factor reflects that actually the broad line contains also a contribution from localized electronic spins such as uncoupled electronic spins localized on Fe ions located within magnetic domains belonging to catalyst residues. Such a result is not unexpected as some iron catalyst particles are embedded within carbon nanotubes during the growth process. The temperature dependence of the g-factor shows an increase with about $20 \pm 1\%$ as the temperature of the sample is decreased from room temperature to liquid nitrogen. This confirms that the broad resonance line is due to conducting (delocalized) electrons interacting weakly with the localized electrons. No significant modifications of the double integral and of the resonance linewidth of the broad line were observed in the temperature range 300–150 K.

The narrow line has not been observed in the ESR spectrum of pristine SWNTs, at room temperature. However, at liquid nitrogen, this narrow and weak line has been noticed at $g = 2.0025 \pm 0.0005$. The rapid increase in the area of this line as the temperature is decreased, confirms its paramagnetic nature. Hence the narrow line originated from paramagnetic impurities is located on carbon nanotubes.

There are no qualitative differences between the ESR spectrum of isolated nanotubes and the resonance spectra of HDPE–SWNTs, at room temperature (see for example Fig. 1a–c). A broad symmetric line with a Lorentzian shape (see Fig. 1a) was observed in HDPE–SWNTs at $g = 2.0725 \pm 0.0005$, at room temperature. The corresponding resonance line in pristine nanotube is located at $g = 2.071 \pm 0.0005$. A faint narrow line superimposed on this broad line was observed (see Fig. 1b) and assigned to paramagnetic impurities. This line is stronger than the line of paramagnetic impurities in pristine SWNTs, and it is located at the same resonance field (within experimental errors), suggesting that the dispersion of nanotubes in polymers resulted in a limited destruction of nanotubes, probably during the sonication step. However, it is not possible to estimate accurately the concentration of paramagnetic defects due to the low amplitude of this line, and to its the convolution with the broad line. An additional wide line originating from ferromagnetic catalysts impurities (iron clusters) was detected at low magnetic fields (see Fig. 1c). To conclude, the ESR spectrum of isolated SWNTs is almost identical to the ESR spectrum of HDPE–SWNTs composites.

The resonance line position, H_R, for an uncoupled electronic spin is correlated to the g-value (assuming that the angular momentum of the electron is quenched) by [21] $h\nu = g\beta H_R$, where h is Planck's constant, ν is the microwave frequency, and β is the Bohr magneton (electron). As it is observed from Fig. 2a and b, the actual g-factor of HDPE–SWNT is larger than the theoretical value for the free electronic spin ($g_0 = 2.0023$) for all resonance lines, in the temperature range 150–450 K. The shift of the g-factor from 2.0023 reflects the combined effect of the interaction between localized and delocalized electrons, spin-orbit coupling, and g-factor anisotropy averaging [1–8] (the actual spectrum is a convolution of resonances corresponding to all orientations of nanotubes relative to the external magnetic field).

From Fig. 2a, it is observed that the g-factor of the broad component ($g^{(B)}$) of the spectrum decreases as the temperature is increased from 150 to about 210 K. This reflects the motional averaging of the g-factor anisotropy derived from the fast enhancement of segmental jump frequencies as the temperature of the polymer is raised above the glass transition temperature, T_G. Hence, the motionally induced averaging of the g-factor is related to the segmental jump frequency and was modeled by a WLF like dependence [23];

$$g = g^* \exp - \frac{C_{1G}(T - T_G)}{T - T_G + C_{2G}} \quad (2)$$

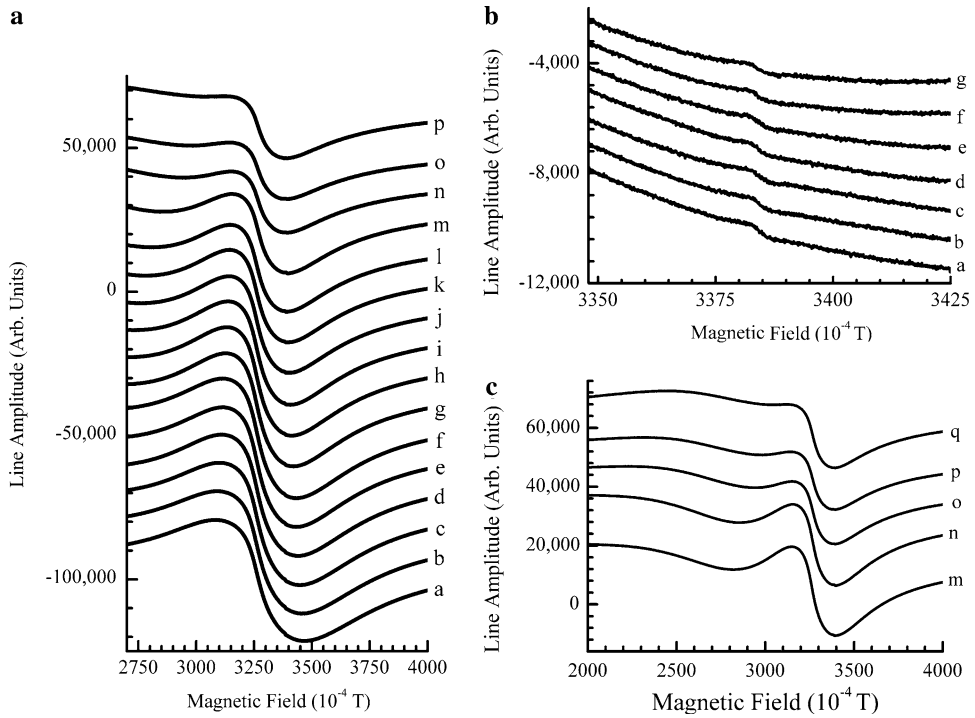

Fig. 1 The resonance spectra of SWNT–PE composites at various temperatures. (**a**) The broad component of the resonance line at various temperatures. (**b**) The faint line component of the resonance line at various temperatures. (**c**) The very broad line (due to catalyst residues) component of the resonance line at various temperatures. These spectra shown in this figure were recorded at the following temperatures: $a = 290$ K; $b = 300$ K; $c = 310$ K; $d = 320$ K; $e = 330$ K; $f = 340$ K; $g = 350$ K; $h = 360$ K; $i = 370$ K; $j = 380$ K; $k = 390$ K; $l = 400$ K; $m = 410$ K; $n = 420$ K; $o = 430$ K $p = 440$ K; $q = 450$ K

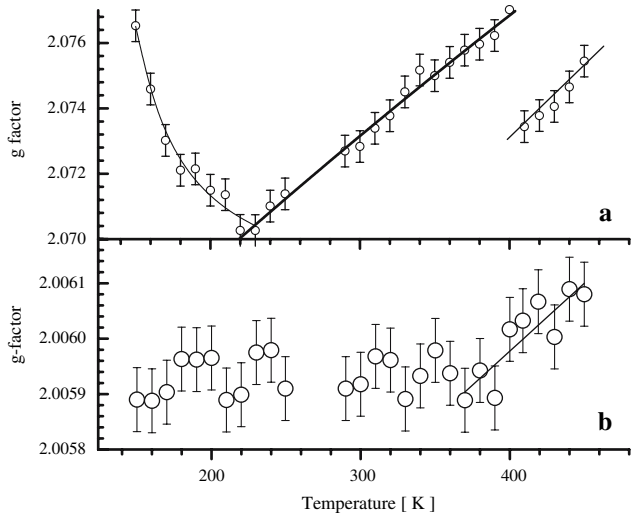

Fig. 2 The temperature dependence of the g-factor for the broad component (g_B, see panel (**a**)) and the narrow component (g_N, see panel (**b**)) of the resonance line. In panel 1, the fine line reflects a WLF like dependence of the g-factor and the solid line represents the best fit obtained within the two-phase approximation

where C_{1G} and C_{2G} are the WLF constants. A good correlation between experimental data and theoretical predictions is observed in the temperature range 150–230 K (see the line in Fig. 2). The best fit was obtained for $g^* = 2.0760 \pm 0.0005$, $C_{1G} = 0.04 \pm 0.01$, $C_{2G} = 35 \pm 5$ K, and $T_G = 150 \pm 10$ K. In conclusion, the dispersion of nanotubes within ultra high-density polyethylene is not affecting the glass transition temperature, within the experimental errors. We may conclude that due to the reduced flexibility of polyethylene chains, these macromolecules are not capable to wrap around carbon nanotubes. The value of C_{1G} is significantly smaller than the expected value for polyethylene (which is of the order of 10 [23]). However, this discrepancy was explained [24] by the fact that, actually the temperature dependence of the g-factor is not directly connected to the free volume but rather proportional to the jump frequency of polymeric chains. Hence, this signal originates from uncoupled electronic spins localized within the polymeric matrix or located at the interface carbon nanotube–polymer. The g-factor of the broad line increases as the temperature is raised above 230 K because the spin bottleneck becomes dominant. This implies the presence of two paramagnetic centers. The temperature dependence of the g-factor in the temperature range 230–400 K was analyzed within the two-phase model [15, 18, 25], which considers the contribution of localized and itinerant electrons,

$$g = (g_{l,B}C_1 + g_{i,B}C_2T)/(C_1 + C_2T)$$

where the subscripts l and i specify localized and itinerant electrons, the subscript B indentifies the broad line, C_1 is proportional to the Curie constant of delocalized electrons, and C_2 [11, 21, 25] to the Fermi susceptibility of itinerant electrons. The best fit was obtained for $g_{i,B} = 2.0605 \pm 0.0005$, $g_{l,B} = 2.1940 \pm 0.005$, and $C_1 = 25 \pm 5$ K and $C_2 = 0.010 \pm .0.005$ (see the bold line in Fig. 2a). A sudden drop in the resonance line position is observed at the melting transition temperature of PE (see Fig. 2a). This fast decrease in the g-factor reflects the fast increase in the segmental jump frequency, which occurs at the melting temperature. By increasing the temperature above 400 K, the bottleneck becomes dominant again, and the g-factor increases as the sample temperature is raised (see Fig. 2a).

The temperature dependence of the narrow line g-factor ($g^{(N)}$) is shown in Fig. 2b. In the temperature range 150–400 K, the g-factor is almost constant. Above the melting temperature, the g-factor starts to increase as the temperature is raised. This behavior suggests that the narrow line originates from paramagnetic entities placed in the crystalline domains of PE or at the interface between crystalline domains and the magnetic ones, or between crystalline domains and carbon nanotubes. However, the errors associated with the deconvolution of the narrow resonance line from the recorded spectrum make difficult an accurate estimation of $g^{(N)}$. From Fig. 2b, it is observed that above the melting temperature of PE (T_{MHDPE}), $g^{(N)}$ increases as the temperature is increased, in agreement with the two-phase approximation. The best fit represented by the bold line corresponds to $g_{i,N} = 2.005 \pm 0.002$, $g_{l,N} = 2.016 \pm 0.008$, and $C_2/C_1 \approx 10^{-4}$ K^{-1}.

The temperature dependence of the peak-to-peak resonance linewidth for the broad component, $H_{PP}^{(B)}$, is shown in Fig. 3a. Several expressions were tested to explain the

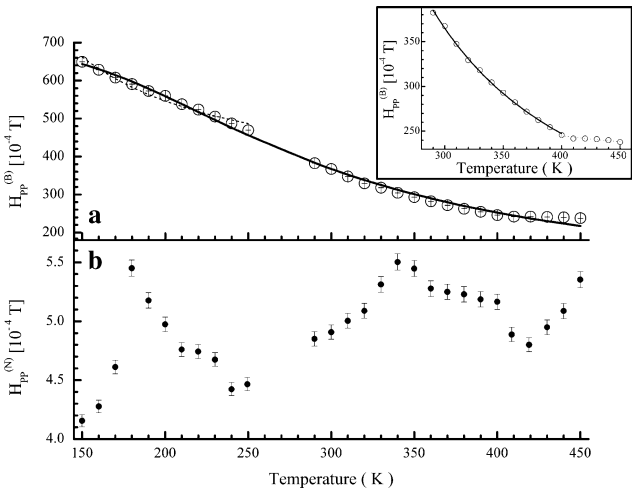

Fig. 3 The temperature dependence of the resonance linewidth for the broad, $H_{PP}^{(B)}$ (see panel (**a**)) and narrow, $H_{PP}^{(N)}$ (see panel (**b**)) components of the resonance line of HDPE–SWNT. The inset shows the departure from the dependence predicted by Eq. 3 above the melting temperature of HDPE

temperature dependence of $H_{PP}^{(B)}$. The Arrhenius like dependence may explain the temperature dependence oh $H_{PP}^{(B)}$ in the temperature ranges 300–400 K and 400–450 K (see in the inset of Fig. 3a the full and dotted lines, respectively). The activation energies associated with the best fit are 0.04 ± 0.005 eV and 0.08 ± 0.01 eV, respectively. The change of the activation energy at 400 K is triggered by the melting of the polymeric matrix. The temperature dependence of $H_{PP}^{(B)}$ in the range 150–300 K is not accurately described by a simple Arrhenius-like dependence (see the dotted line in Fig. 3a). The two-phase approximation [18, 25] predicts the following temperature dependence for H_{PP};

$$H_{PP}^{(B)} = \frac{pH_{PP}^{l}}{p + (1-p)\,\exp -E_A/K_BT} + \left[\frac{(1-p)H_{PP}^{i}}{p + (1-p)\,\exp -E_A/K_BT}\right] \quad (3)$$

where the subscripts l and i identify the localized and itinerant contributions to the linewidth, p is the concentration of traps, and E_A is the activation energy from the trap. From Fig. 3a, it is observed that this expression provides the best fit of experimental data (see the bold line). The corresponding parameters are $p = 0.070 \pm 0.005$, $E_A = 0.070 \pm 0.005$ eV, $H_{PP}^{l} = 67 \pm 1$ mT, and $H_{PP}^{i} = 0.03 \pm 0.005$ mT. Equation 3 explains accurately the temperature dependence of $H_{PP}^{(B)}$ from 150 K to T_{MHDPE}. Above this temperature, the traps disappear ($p = 0$) and the dependence degenerates into a simple Arrhenius like dependence. The temperature dependence of $H_{PP}^{(N)}$ for the faint line is complex (see Fig. 3b). The decrease in $H_{PP}^{(N)}$ as the temperature is increased from 180 to 250 K reflects a motional narrowing of the resonance line due to the enhancement of molecular motions above the glass transition temperature of PE (T_{GHDPE}). The decrease of $H_{PP}^{(N)}$ as the temperature is increased from 340 to 410 K is associated with PE melting. The melting of crystallites allows for faster reorientations and rotations of nanotubes, narrowing the resonance line. Above T_{MHDPE}, the dramatic enhancement of macromolecular motions should decrease further the resonance linewidth. The bottleneck of spin relaxation is responsible for the broadening of the resonance line observed above T_{MHDPE}. A bottleneck of the complex relaxation that involves both localized and itinerant electrons is responsible for the temperature dependence of $H_{PP}^{(N)}$ in the range 240–340 K.

The double integral of the resonance lines, S, was estimated by using $S = KIH_{PP}^2/(mA)$, where I is the resonance line amplitude, K is a constant related to the resonance line shape, m is the mass of the sample, and A is the spectrometer's gain. S is proportional to the spin susceptibility of the sample [11]. For the electrons residing on conducting nanotubes, the expected temperature dependence is

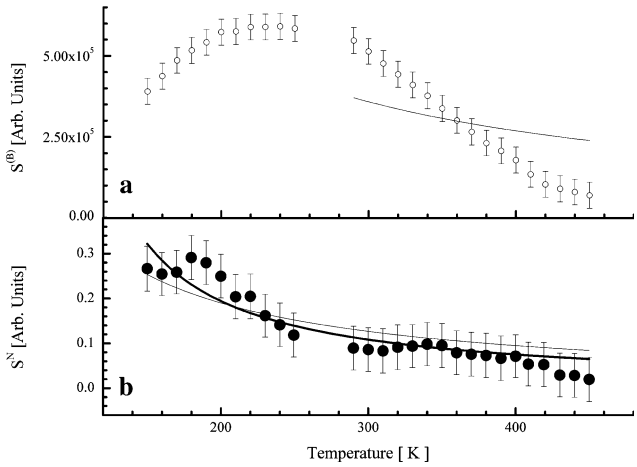

Fig. 4 The temperature dependence of the parameter S for the broad component ($S^{(B)}$, see panel (**a**)) and for the narrow component ($S^{(N)}$, see panel (**b**)) of the resonance line parameters for the faint line. The fine line in both panels corresponds to pure paramagnetic contributions. The bold line in the bottom panel describes a mixture of uncoupled electronic spins (paramagnetic) interacting via exchange interactions with a small amount of electrons delocalized over conducting domains

$S = C_1 + C_2/T$ [11–14]. From Fig. 4a it is observed that $S^{(B)}$ (B identifies the broad component) increases as the temperature is increased from 150 to 220 K. This is at variance with the expected temperature dependence of paramagnetic (see the line in Fig. 4a) or conducting phases, and may be explain either by the thermally induced generation of uncoupled electronic spin or by a more complex structure of the energy levels involving an effective spin $s > 1/2$ [21]. The temperature dependence of $g^{(B)}$ and $H_{PP}^{(B)}$ does not support an effective spin $s > 1/2$. The temperature dependence of $H_{PP}^{(B)}$, is consistent with a thermally induced de-trapping of electrons. In the temperature range 230–450 K, $S^{(B)}$ decreases as the temperature is increased. The temperature dependence of the double integral of the narrow component of the resonance spectrum, $S^{(N)}$, is shown in Fig. 4b. Excepting a local maximum at about 180 K, $S^{(N)}$ decreases as the temperature of the sample is increased. Such dependence is typical for a paramagnetic system. The line in Fig. 4b represents a Curie (pure paramagnetic) fit of the dependence of $S^{(N)}$ on temperature, in the range 300–400 K. A weak temperature independent contribution is also possible. The reduced amplitude of the narrow line and the errors due to the convolution of the broad and narrow components preclude a more accurate analysis of the temperature dependence of the narrow line parameters.

Conclusions

ESR investigations on HDPE–SWNT revealed a complex resonance spectrum consisting of three lines:

1. A wide resonance line with a g-factor higher than 2.1, was observed and assigned to magnetic iron clusters (catalyst residues). The parameters of this line are temperature dependent; this reflects the fact that the uncoupled electronic spins are subjected to both internal and external magnetic fields.
2. A broad line localized near the free electron g-value and assigned to conducting electrons delocalized over the conducting domains of carbon nanotubes. The temperature dependence of the resonance line parameters belonging to the broad line is consistent with a two-phase model suggesting strong interactions between the localized electronic spins residing on carbon nanotubes and the itinerant electronic spins located on magnetic impurities (catalysts residues). The broad line contains information concerning the SWNT–HDPE interface.
3. A narrow line with a strong (Curie like) temperature dependence assigned to paramagnetic defects located on carbon nanotubes. The position of the narrow line confirms that the uncoupled electronic spins from paramagnetic impurities (such as amorphous carbon) contribute to this resonance. The complex behavior of $H_{PP}^{(N)}$ indicates that the uncoupled electronic spins are located at the interface between crystalline and amorphous domains of the polymeric matrix (HDPE), and are originating from amorphous carbon or graphite residues floating within the polymeric matrix.

Acknowledgements This work was supported by NSF Grant # DMR 0606224 (University of Texas pan American), NASA # NCC-01-0203 Grant and NCC-9-114 (Rice University), and US ARMY STTR #A2-1299 grant. The STTR #A2 1299 grant has been awarded to the Chemistry Department of Indiana University (Bloomington) and to PartTec Ltd.

References

1. Salvetat-Delmotte JP, Rubio A (2002) Carbon 40(10):1729
2. Lau KT, Hui D (2002) Compos Part B: Eng 33(4):263
3. Lau KT, Hui D (2002) Carbon 40(9):1605
4. Lau KT, Chipara M, Hui D (2004) Compos Part B: Eng 35(2):95
5. Rafii-Tabar H (2004) Phys Rep 390(4–5):235
6. Ju S. Li ZY (2006) Phys Lett A 353(2–3):194
7. Yamamoto T, Watanabe S, Watanabe K (2004) Thin Solid Films 464–465:350
8. Kaiser AB, Challis KJ, McIntosh GC, Kim GT, Yu HY, Park JG, Jhang SH, Park YW (2002) Curr Appl Phys 2(2):163
9. Mayer A, Lambin Ph (2002) Carbon 40(3):429
10. Chipara M, Lozano K, Chipara MD (2007) Carbon 45(13):2698
11. Petit P, Jouguelet E, Fischer JE, Rinzler AG, Smalley RE (1997) Phys Rev B 56(15):9275
12. Shen K, Thierney DL, Pietrass T (2003) Phys Rev B 68:165418
13. Yokomichi H (2004) Vacuum 3–4(7):677
14. Chipara M, Zaleski JM, Iacomi F, Bai JB (2006) J Optoelectr Adv Mat 8(2):820
15. Likodimos V, Glenis S, Guskos N, Lin CL (2003) Phys Rev B 68:045417
16. Garaj S, Thien-Nga L, Gaal R, Forro L, Takahashi K, Kokai F, Yudasaka M, Iijima S (2000) Phys Rev B 62(24):17115
17. Chipara M, Zaleski JM, Hui D, Du C, Pan N (2005) J Polym Sci Polym Phys 43:3406
18. Arcon D, Zorko A, Cevc P, Mrzel A, Remskar M, Dominko R, Gaberscek M, Mihailovic D (2003) Phys Rev B 67:125423
19. Gutsev GL, Bauschlicher CW, Andrews L (2003) J Chem Phys 119(7):3681
20. Yang CM, Kaneko K, Yudasaka M, Iijima S (2002) Physica B-Cond Matt 323(1–4):140
21. Kittel Ch (1996) Introduction to solid state physics. John Wiley & Sons, New York
22. Pulikkathara MX, Shofner ML, Wilkins R, Vera JG, Barrera EV, Rodriguez-Macias FJ, Vaidyanathan RK, Green CE, Condon CG (2003) Mat Res Soc Symp Proc 740:365
23. Davis GT, Eby RK (1973) J Appl Phys 44(10):4274
24. Chipara M (1997) Physica B 234–236:263
25. Beuneu F, l'Huilier C, Salvetat JP, Bonard JM, Forro L (1999) Phys Rev B 59(8):5945